ARTICLES
PUBLISHED ONLINE: 8 MARCH 2009 | DOI: 10.1038/NPHYS1220
nature physics

One-dimensional topologically protected modes in topological insulators with lattice dislocations

Ying Ran[1,2]*, Yi Zhang[1] and Ashvin Vishwanath[1,2]

Topological defects, such as domain walls and vortices, have long fascinated physicists. A novel twist is added in quantum systems such as the B-phase of superfluid helium He_3, where vortices are associated with low-energy excitations in the cores. Similarly, cosmic strings may be tied to propagating fermion modes. Can analogous phenomena occur in crystalline solids that host a plethora of topological defects? Here, we show that indeed dislocation lines are associated with one-dimensional fermionic excitations in a 'topological insulator', a novel phase of matter believed to be realized in the material $Bi_{0.9}Sb_{0.1}$. In contrast to fermionic excitations in a regular quantum wire, these modes are topologically protected and not scattered by disorder. As dislocations are ubiquitous in real materials, these excitations could dominate spin and charge transport in topological insulators. Our results provide a novel route to creating a potentially ideal quantum wire in a bulk solid.

Motivated by applications to spintronics, recent theoretical work on the effect of spin–orbit interactions on the band structure of solids predicted the existence of novel 'topological insulators' in two[1–3] and three dimensions[4–6]. In two dimensions, these new insulators strongly resemble the quantum Hall states, although there are no applied magnetic fields, and time-reversal symmetry is preserved. Although there is an excitation gap in the bulk as in conventional band insulators, there are gapless modes at the edge, which appear in time-reversed pairs with opposite spin and velocity. Transport measurements on HgCdTe quantum wells[7,8] have provided evidence for the existence of these 'helical' edge states[1,9,10]. In three dimensions, topological insulators are classified as strong ($\nu_0 = 1$) or weak ($\nu_0 = 0$); the former has surface states with an odd number of Dirac points, which cannot be realized in two-dimensional (2D) band structures with time-reversal symmetry. In addition, 3D topological insulators are characterized by indices (ν_1, ν_2, ν_3) with respect to a basis of reciprocal lattice vectors $(\mathbf{G}_1, \mathbf{G}_2, \mathbf{G}_3)$. These essentially serve to define a time-reversal-invariant momentum (TRIM) $\mathbf{M}_\nu = (1/2)(\nu_1\mathbf{G}_1 + \nu_2\mathbf{G}_2 + \nu_3\mathbf{G}_3)$. The recent prediction[4] and evidence from angle-resolved photoemission experiments[11] for a strong topological insulator phase in the alloy $Bi_{0.9}Sb_{0.1}$, has led to heightened interest in these systems. Weak topological insulators are entirely characterized by $\mathbf{M}_\nu \neq 0$, and can be obtained by stacking layers of 2D topological insulators along the $\mathbf{M}_\nu$ direction. It is sometimes stated that even weak disorder will immediately wipe out the weak topological insulator. However, as argued at the end of this article, a more careful consideration on the basis of the results here points to a different conclusion. For the present, we will assume crystalline long-range order.

Dislocations are line defects of the 3D crystalline order, characterized by a vector $\mathbf{B}$ (the Burgers vector), which is a lattice vector. This is rather like the quantized vorticity of a superfluid vortex, and must remain constant over its entire length. The centre of the dislocation is at $\mathbf{R}(\sigma)$ where σ parameterizes the line defect. A convenient way to visualize a dislocation is through the Volterra process. One begins with the perfect crystal and chooses a plane P that terminates along the curve $\mathbf{R}(\sigma)$ where the defect is to be produced. The crystal on one side of the plane P is then displaced by the lattice vector $\mathbf{B}$, and extra atoms are inserted or removed if required. At the end, crystalline order is restored everywhere except near the curve $\mathbf{R}(\sigma)$. A screw dislocation (see Fig. 1a) is a straight line defect that runs parallel to its Burgers vector, that is, the tangent vector $\mathbf{t} = \mathrm{d}\mathbf{R}(\sigma)/\mathrm{d}\sigma$ is constant, and $\mathbf{t} \parallel \mathbf{B}$, whereas an edge dislocation is also a straight line defect that runs perpendicular to the Burgers vector $\mathbf{t} \perp \mathbf{B}$. In general, a dislocation varies between these two simple types along its length, depending on the orientation of its tangent vector relative to the Burgers vector.

With these preliminaries, our results are readily stated. Consider a 3D topological insulator characterized by $\nu_0, \mathbf{M}_\nu$, and insert a dislocation along $\mathbf{R}(\sigma)$ with the Burgers vector $\mathbf{B}$. Then, if

$$\mathbf{B} \cdot \mathbf{M}_\nu = \pi \,(\mathrm{mod}\, 2\pi) \tag{1}$$

the dislocation induces a pair of 1D modes bound to it, which propagate in opposite directions and traverse the bulk bandgap. They closely resemble the helical modes at the edge of a 2D quantum spin Hall insulator. Once established, they are protected by time-reversal symmetry and the bulk energy gap, and reflect the non-trivial topology of the band structure. Although a trivial insulator could also develop 1D propagating modes along a dislocation, the precise count obtained here—a single Kramers pair of propagating modes—cannot arise. The topological stability of a single pair of modes results from time-reversal symmetry, which prohibits backscattering between the oppositely propagating 1D modes[2]. From equation (1), we note that some dislocations, for example, with $\mathbf{B} \perp \mathbf{M}_\nu$, do not carry these helical modes. In addition, there is the 'pristine' strong topological insulator $\nu_0 = 1, \mathbf{M}_\nu = 0$, where none of the dislocations induces helical modes. Note that $Bi_{0.9}Sb_{0.1}$, which experiments indicate is a topological insulator, is characterized by $\nu_0 = 1$ and a non-trivial $\mathbf{M}_\nu$, which connects the Γ and T points in the Brillouin zone. We will later comment on experimental consequences arising from the dislocation-induced helical liquids in this material. In this work, we focus on dislocations; the electronic properties of other defects (for example, domain walls,

[1]Department of Physics, University of California, Berkeley, California 94720, USA, [2]Materials Sciences Division, Lawrence Berkeley National Laboratory, Berkeley, California 94720, USA. *e-mail: ranying@berkeley.edu.

© 2009 Macmillan Publishers Limited. All rights reserved.

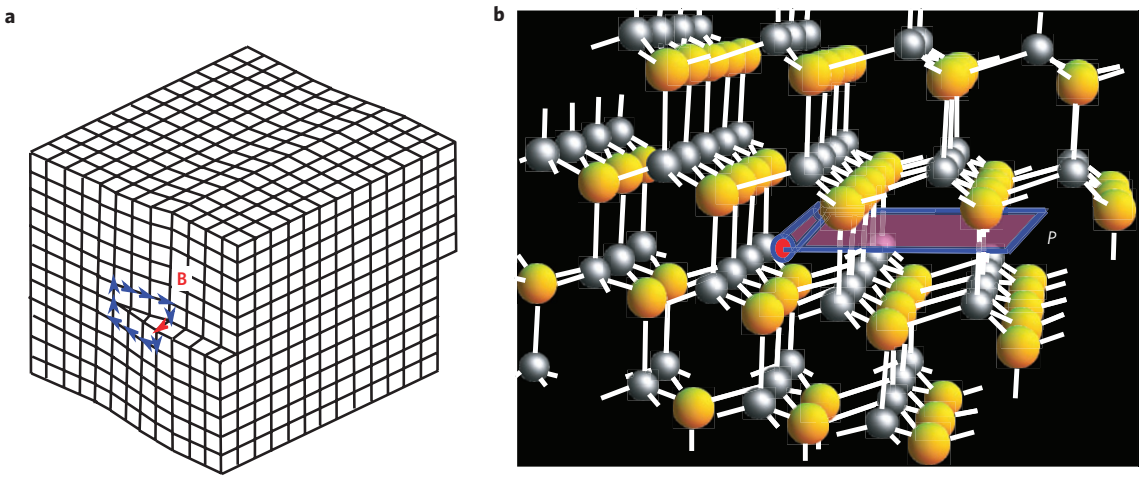

Figure 1 | Screw dislocations. a, Cubic-lattice screw dislocation with the Burgers vector **B**. **b**, Diamond-lattice screw dislocation along the $\mathbf{B} = a(1,1,0)$ direction (shown as a cylinder with red ends), studied in the text. The two diamond sublattices are shown as yellow and white spheres. A cutting plane P that was used to generate the dislocation is shown, orthogonal to the strength t nearest-neighbour bond along $a/2(1,-1,-1)$.

see ref. 12 for an early discussion of these in PbTe semiconductors) are left to future work.

Dislocations in the diamond-lattice topological insulator

Instead of plunging into a general proof of our results, we first present a numerical calculation of the electronic structure of a dislocation in a simple realization of a topological insulator, which vividly shows our central result equation (1). Following ref. 4, we consider a tight-binding model on the diamond lattice with nearest-neighbour hopping, and spin–orbit-induced next-nearest-neighbour hopping:

$$H = t\sum_{\langle ij\rangle} c^{\dagger}_{i\sigma}c_{j\sigma} + i\frac{8\lambda_{\mathrm{SO}}}{(2a)^2}\sum_{\langle\langle ik\rangle\rangle} c^{\dagger}_{i\sigma}(\mathbf{d}^1_{ik}\times\mathbf{d}^2_{ik})\cdot\boldsymbol{\sigma}_{\sigma\sigma'}c_{k\sigma'} \qquad (2)$$

where $c_{i\sigma}$ is the electron operator of spin σ at site i, t is the nearest-neighbour hopping amplitude, λ_{SO} is the spin–orbit-induced next-nearest-neighbour hopping amplitude, $\mathbf{d}^1_{ik}, \mathbf{d}^2_{ik}$ are the two nearest-neighbour bond vectors leading from site i to k, $\boldsymbol{\sigma}$ are the spin Pauli matrices and $2a$ is the cubic cell size. The system is a Dirac metal at this point, and a full gap is opened on distorting the lattice, by making the nearest-neighbour hopping strengths $t+\delta t$ along one of the directions, such as $(a/2)(1,1,1)$. If $\delta t > 0$ ($\delta t < 0$), the system is a strong (weak) topological insulator with $\nu = 1$ ($\nu = 0$) and $\mathbf{M}_\nu = (\pi/2a)(1,1,1)$. We now introduce a dislocation. For numerical convenience we study a screw dislocation, which is simple to model, and use periodic boundary conditions—which requires us to consider a pair of (separated) dislocations. Translation symmetry is present along the dislocation axis, and we label states by the crystal momentum (k) in this direction. The precise geometry we use is shown in Fig. 1b. If $\mathbf{a}_1 = a(0,1,1)$, $\mathbf{a}_2 = a(1,0,1)$, $\mathbf{a}_3 = a(1,1,0)$ represent the diamond-lattice basis vectors, the dislocations are along the $\mathbf{a}_3$ axis. A screw dislocation is readily implemented in a tight-binding model as follows. The bonds cut by the imaginary plane shown in Fig. 1b, which are moved to connect to the next layer of atoms, have their hopping amplitudes changed by $t \to te^{\pm ik\hat{k}\cdot\mathbf{B}}$.

For a pair of unit screw dislocations $\mathbf{B} = a(1,1,0)$ in this direction, we find four 1D modes, two down-moving and two up-moving modes, within the bulk gap (Fig. 2a). The wavefunctions of these modes are peaked along the two dislocations (Fig. 2c)—hence, a pair of oppositely propagating modes is present for each dislocation line. The modes are time-reversal (Kramers) conjugates of each other. Not all dislocations carry these gapless modes—if we double the Burgers vector of this dislocation (Fig. 2b), or consider a different relative orientation when the unequal bond is orthogonal to the Burgers vector (Fig. 2d), the 1D modes do not appear. The sign of δt, however, is immaterial—both weak and strong topological insulators show this physics.

For an isolated dislocation, these time-reversed 1D modes are topologically protected, and can be removed only if the bandgap in the bulk of the crystal closes, or if time-reversal symmetry is broken. This enables us to immediately deduce the following result. The condition for a gapless line mode to exist on a dislocation cannot depend on its orientation, as it must propagate through the entire defect. Hence, it can depend only on the Burgers vector **B**, which remains constant through the entire length of the dislocation. Therefore, although we have explicitly considered the case of a screw dislocation, the result also holds for an edge or mixed dislocation with the same Burgers vector.

We now present an analytical rationalization for the existence of gapless modes along the dislocation line, in this model of the strong topological insulator. We study the model in a limit that is analytically tractable, but nevertheless adiabatically connected to the parameter regime of interest. Consider the imaginary plane P (orthogonal to $(1,-1,-1)$), used to construct the dislocation, which ends along the dislocation line. Extend this plane through the entire crystal, weakening all bonds that are cut by it. This plane cuts the strength t nearest-neighbour bonds, which run along the $(1,-1,-1)$ direction. Now, the crystal is almost disconnected into two disjoint pieces. The disconnected crystal has gapless states on the two surfaces S_+, S_- that are created, with a single Dirac node located at the surface momentum $\mathbf{m}_{\mathrm{D}} = (\pi/2a)(1,1,0)$. Electronic states in the vicinity of the Dirac point can be expanded as $\Psi(x_1,x_2) \sim e^{i\mathbf{m}_{\mathrm{D}}\cdot\mathbf{x}}\psi(\mathbf{x})$, where $\psi(\mathbf{x})$ varies slowly over a lattice spacing. The effective Hamiltonian for such states on the two surfaces is $\pm H_0$ (ref. 4), with:

$$H_0(p) = v_1 p_1 \hat{n}_1\cdot\boldsymbol{\sigma} + v_2 p_2 \hat{n}_2\cdot\boldsymbol{\sigma}$$

where p_1, p_2 are surface momenta measured from the Dirac point, with p_1 along the dislocation line (the $(1,1,0)$ direction) and p_2 orthogonal to it. The $\boldsymbol{\sigma}$ are the spin Pauli matrices and $\mathbf{n}_{1,2}$ are two linearly independent unit vectors. Thus, if $\mu_z = \pm 1$ represents the two surfaces, the effective Hamiltonian is $H = H_+(p)\mu_z$. Now, if we imagine reconnecting the surfaces without creating a dislocation, we add a hopping term (m) between

© 2009 Macmillan Publishers Limited. All rights reserved.

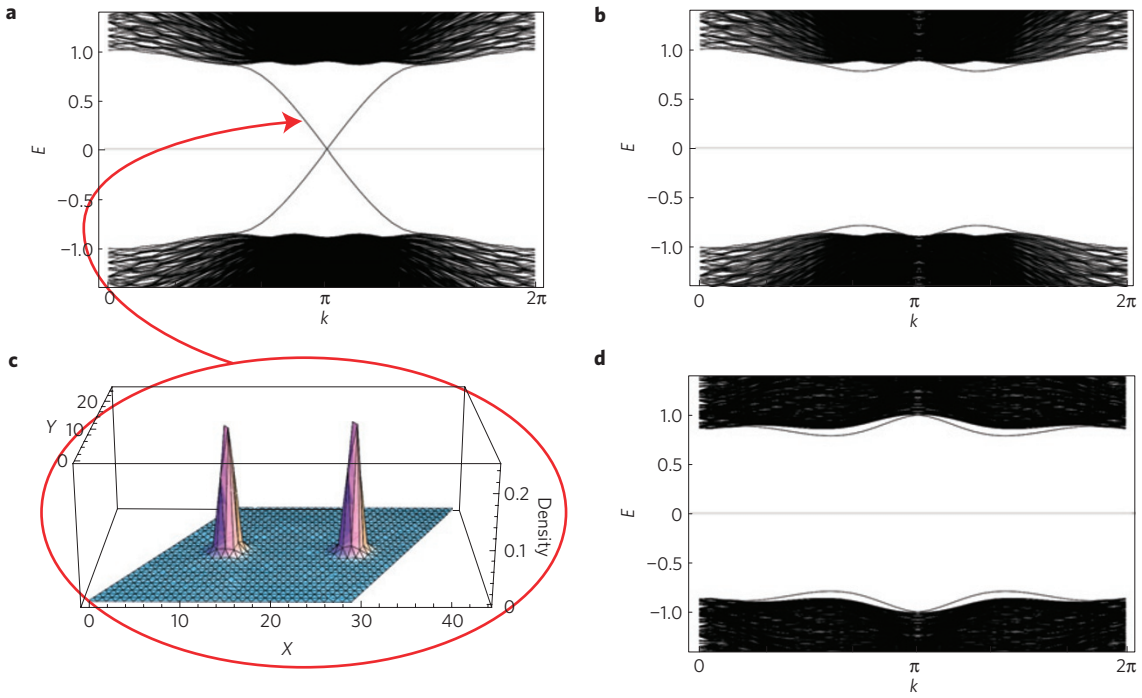

Figure 2 | Dislocation-induced electronic states. Spectrum of the diamond-lattice strong topological insulator ($\mathbf{M}_\nu = (\pi/2a)(1,1,1)$) in the presence of a pair of screw dislocations. Electronic states are shown as a function of k, the wave vector along the dislocation. For **a**–**c**, the dislocations are oriented along the $\mathbf{a}_3 = a(1,1,0)$ axis. **a**, Spectrum, when the dislocation Burgers vector $\mathbf{B} = \mathbf{a}_3$ and satisfies $\mathbf{B}\cdot\mathbf{M}_\nu = \pi$. A pair of counterpropagating modes per dislocation is found, which span the bandgap (each midgap level happens to be doubly degenerate). **b**, Spectrum when $\mathbf{B} = 2\mathbf{a}_3$ and $\mathbf{B}\cdot\mathbf{M}_\nu = 0 \pmod{2\pi}$. No dislocation modes occur. **c**, Probability distribution of a pair of midgap modes shown in the $\mathbf{a}_1, \mathbf{a}_2$ plane that intersects the dislocations. The modes are bound near the dislocations. **d**, The dislocations are oriented along $\mathbf{B} = a(0,1,-1)$ and $\mathbf{B}\cdot\mathbf{M}_\nu = 0$. No dislocation modes occur. Calculations were done on a $36 \times 36 \times 18$ unit-cell system with periodic boundary conditions along $\mathbf{a}_1, \mathbf{a}_2, \mathbf{B}$ directions, and dislocations separated by a half system size. The hopping parameters used in equation (2) are $t = 1$, $t + \delta t = 2$ and $\lambda_{SO} = 0.125$.

the two surfaces: $H = H_+(p)\mu_z + m\mu_x$, which leads to fully gapped dispersion, with gap $2m$, which can be adiabatically connected to the uniform bulk insulator.

Now consider introducing a screw dislocation, by displacing the surface to one side of the plane P by the lattice vector $\mathbf{B} = a(1,1,0)$. Reconnecting the bonds is now described as follows. In our surface coordinate system, the dislocation line is along the x_1 axis, at $x_2 = 0$, and the plane P is at $x_2 > 0$. The crucial observation is that when reconnecting the bonds across the plane P, the Dirac particles acquire a phase shift of $e^{i\mathbf{m}_D\cdot\mathbf{B}} = -1$ as the Dirac node is located at the specific wave vector $\mathbf{m}_D$, which when displaced by the Burgers vector $\mathbf{B}$ leads to a π phase shift. The effective Hamiltonian in the presence of a dislocation is then:

$$H_{\rm dis} = H_+(-i\hbar\nabla)\mu_z + m(x_2)\mu_x$$

where the Dirac mass term is now position dependent: $m(x_2 < 0) = m$ but $m(x_2 > 0) = -m$. Such Dirac Hamiltonians are well known to lead to low-energy modes that are protected by index theorems[13]. We explicitly demonstrate this below.

As p_1 is a good quantum number, consider first the Hamiltonian at $p_1 = 0$. $H_{\rm dis}(p_1 = 0) = v_2\hat{n}_2\cdot\boldsymbol{\sigma}\mu_z(-i\hbar\partial_{x_2}) + m(x_2)\mu_x$. Such a 1D Dirac equation is well known to have a zero-energy state[14]:

$$\psi(x_2) = e^{\frac{1}{\hbar v_2}\int_0^{x_2} dx_2 m(x_2)}\psi_0$$

where ψ_0 satisfies: $\mu_y\hat{n}_2\cdot\boldsymbol{\sigma}\psi_0 = +\psi_0$. As $m(x_2 \to +\infty) < 0$ and $m(x_2 \to -\infty) > 0$, the state is normalizable. In fact, there is a Kramers pair of degenerate states present. The dispersing 1D modes are obtained by studying the splitting of this pair, on changing the momentum p_1. For small momenta, this leads to the effective Hamiltonian $H_{\rm eff} = v_1 p_1 \mathbf{n}_{1\perp}\cdot\sigma\mu_z$, where $\mathbf{n}_{1\perp} = \hat{n}_2 \times (\hat{n}_1 \times \hat{n}_2)$, which leads to a pair of counterpropagating 1D modes with linear dispersion $\epsilon(p_1) = \pm v_1 p_1\sqrt{1-\hat{n}_1\cdot\hat{n}_2}$ that are confined to the dislocation.

These 1D modes span the bandgap, connecting the filled and empty bands. As long as time-reversal symmetry is present, a single pair of them cannot acquire a gap[2], which makes them a defining property of the phase. Note, the crucial step in the derivation of the 1D modes above, was the fact that the low-energy surface states on the cut surface were at the non-trivial surface momentum $\mathbf{m}_D$, such that $\phi = \mathbf{B}\cdot\mathbf{m}_D = \pi$. More generally, if there are several such surface Dirac modes $\mathbf{m}_D^i$, what is required is that an odd number of them acquire a π phase shift on circling the dislocation $\sum_i \mathbf{m}_D^i\cdot\mathbf{B} = \pi \pmod{2\pi}$. This guarantees the existence of at least a pair of gapless 1D modes on the dislocation. If on the other hand, $\sum_i \mathbf{m}_D^i\cdot\mathbf{B} = 0 \pmod{2\pi}$, there are no protected modes on the dislocation. Indeed, this occurs in the model above if, for example, we choose the $\mathbf{B}$ orthogonal to the $(1,1,1)$ direction (the direction of the strong bond).

Dislocations in a general topological insulator

Armed with these insights for a specific model, one may discuss the general case of an arbitrary dislocation in a topological insulator, and when a protected 1D gas is expected to occur. For a topological insulator characterized by $\{\nu_0, \mathbf{M}_0\}$, and a dislocation with the Burgers vector $\mathbf{B}$, the condition for the existence of a protected 1D mode is given by equation (1), and derived in the general case in the Methods section.

For the weak topological insulator case, however, a more intuitive derivation of this result is possible. The weak topological insulator is adiabatically connected to a stack of decoupled 2D

© 2009 Macmillan Publishers Limited. All rights reserved.

topological insulators, stacked along the $\mathbf{M}_\nu$ direction. The top and bottom surfaces of the stack are fully gapped. Consider creating a screw dislocation in such a stack, by cutting and regluing layers in the manner shown in Fig. 3. Cutting a plane results in a pair of edge modes, which are gapped after the planes are glued back together. However, edge modes in the top and bottom layers are left out in this process—just one member of the counterpropagating edge mode pair is shown in the figure. As a single pair of such modes cannot begin or end, they must propagate through the dislocation core to complete the circuit. Thus, helical dislocation modes must occur in this set-up. Similarly, an edge dislocation created by inserting an extra half-plane in this layered set-up will carry protected edge modes. Note, such a graphical derivation is not feasible for a strong topological insulator, where no 2D limit exists. For a 3D Chern insulator[15], characterized by a reciprocal lattice vector $\mathbf{G}_0$, a dislocation line should have $(\mathbf{G}_0 \cdot \mathbf{B}/2\pi)$ chiral modes propagating along it.

It is sometimes stated that in the presence of disorder, only the ν_0 index is robust, whereas the $\mathbf{M}_\nu$ index is irrelevant. Hence, weak topological insulators, of which the surface states can be localized, are believed to be unstable to disorder[4]. As our results pertain to a distinct topological property controlled by the $\mathbf{M}_\nu$ index, they shed light on the stability of weak topological insulators. For sufficiently weak disorder, the system stays insulating and dislocations are expected to remain well defined (discussed in more detail below). Then, the helical edge modes accompanying the relevant dislocations continue to be protected, which means that the $\mathbf{M}_\nu$ index, and weak topological insulators, remain well defined. When can dislocations be meaningfully defined in a disordered crystal? Crystalline long-range order is a sufficient condition, as the local order parameter can then be used to define dislocations. In some cases, even in the absence of long-range order, dislocations may be well defined—for example, the Bragg glass phase has only algebraic order, but dislocations are not proliferated[16]. Certainly, in real crystals, which are inevitably disordered, dislocations are

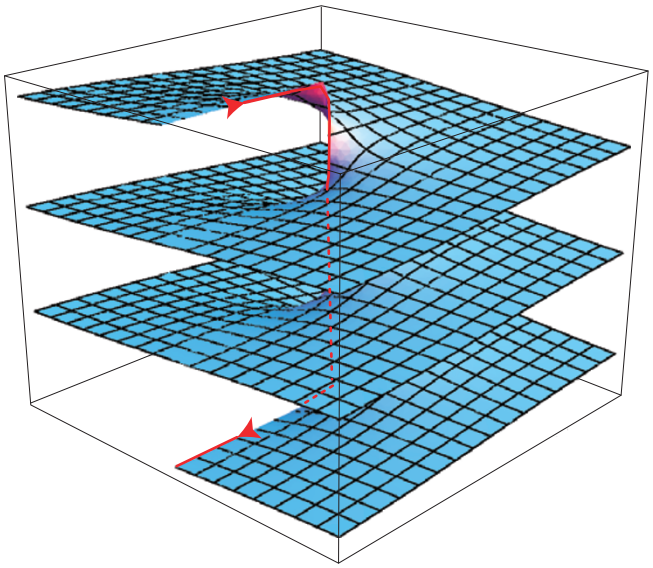

Figure 3 | Screw dislocation in a weak topological insulator. The unpaired edge modes (one member of the edge mode pair is shown in red) of the top and bottom layer must propagate through the dislocation by continuity.

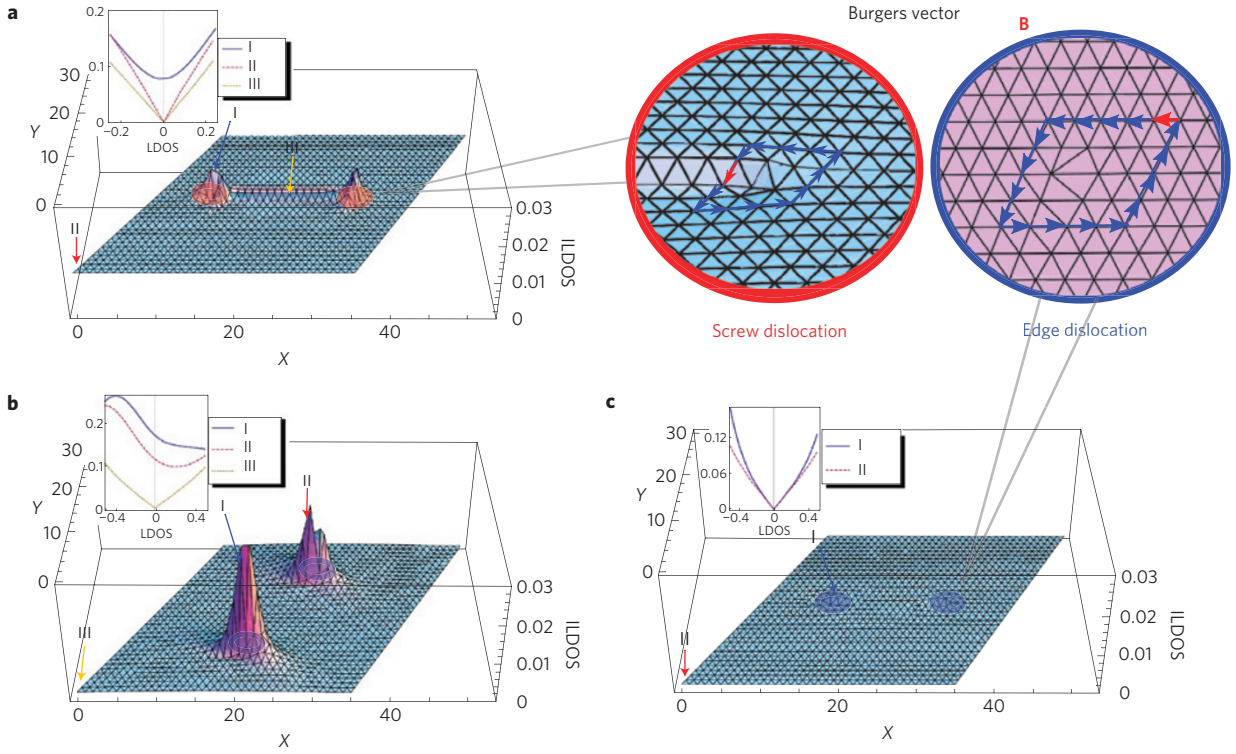

Figure 4 | Surface DOS in the presence of dislocations. LDOS as measured by STM, for various dislocation configurations, in the diamond-lattice strong topological insulator with parameters as in Fig. 2. In all cases, dislocation pairs are separated by a half system size (and are directed along $\mathbf{a}_3$). The topography of the integrated LDOS (ILDOS) in the energy window $[-0.1, 0.1]$ is shown, with insets showing energy-dependent LDOS at special points on the surface. **a**, The (111)′ surface intersecting a pair of screw dislocations with $\mathbf{B} = a(1,1,0)$. These carry 1D modes that give rise to a peak in the integrated LDOS. **b**,**c**, Edge dislocations on the $(\bar{1}\bar{1}1)$ surface. In **b**, the dislocation satisfies $\mathbf{B} \cdot \mathbf{M}_\nu = \pi$, and has 1D modes visible in the LDOS, whereas in **c**, the dislocation has $\mathbf{B} \cdot \mathbf{M}_\nu = 0$, hence no 1D line mode and no enhanced LDOS. In **a**–**c**, only the top layer of atoms is shown, and calculations are done on a $36 \times 36 \times 18$ unit-cell system, with periodic boundary conditions in the $\mathbf{a}_1, \mathbf{a}_2$ directions.

© 2009 Macmillan Publishers Limited. All rights reserved.

well-defined objects, and hence the physics discussed in this article should apply. However, if disorder is so strong that the dislocations are no longer well defined, then the only remaining distinction is the ν_0 index. Similarly, an insulator with $\mathbf{M}_\nu \neq 0$ can be converted to one with $\mathbf{M}_\nu = 0$, by introducing a potential modulation with period $\mathbf{M}_\nu$. Elementary dislocations that carry helical modes will then cost infinite energy per unit length.

Experimental consequences

In real solids, dislocations are always present and the predicted helical modes should have important experimental consequences. Scanning tunnelling microscopy (STM) of a topological insulator surface where dislocations terminate, is particularly well suited to verify these predictions. As the precise atomic arrangement is visualized by STM, the nature of the dislocations involved can be characterized. At the same time, the finite density of states (DOS) associated with the 1D modes will lead to an enhanced tunnelling DOS near the dislocation core. This will be particularly striking if one tunes to an energy where the surface modes contribute minimally (for example, at the Dirac node). Such experiments are immediately feasible on the putative topological insulator $Bi_{0.9}Sb_{0.1}$ with A7 structure. As the band structure of that material is complex and still debated[17], we demonstrate qualitatively what is expected, in the simpler diamond-lattice strong topological insulator model (2). Moreover, as the crystal symmetries in the two cases share several features—such as a three-fold axis parallel to the $\mathbf{M}_\nu$ vector, some predictions for the diamond-lattice model may be directly relevant to the A7 structure. First, consider the surface orthogonal to the strong bond $(1,1,1)$ direction. We choose this surface to cut three strength t bonds (rather than a single strong bond) to obtain a surface band structure similar in some respects to the (111) surface of $Bi_{0.9}Sb_{0.1}$. We call this the $(111)'$ surface. This surface has a single Dirac node centred at the Γ point in the surface Brillouin zone. We consider a pair of separated screw dislocations with $\mathbf{B} = a(1,1,0)$, which carry 1D helical modes, that terminate on the surface. STM measures the local DOS (LDOS) at a given energy and surface location $\rho(\mathbf{r}, E) = \sum_\alpha |\psi_\alpha(\mathbf{r})|^2 \delta(E - E_\alpha)$, where the α sum runs over all eigenstates. The dislocations appear as peaks in the LDOS as shown in Fig. 4a, owing to these 1D modes. Note, the ledge connecting the two screw dislocations on the surface also shows an enhanced DOS.

More striking evidence for the relation (1) appears when we consider the edge dislocations on the $(\bar{1}\bar{1}1)$ surface. If the Burgers vector of the dislocation is $\mathbf{B} = a(1,0,1)$ the 1D modes are present (Fig. 4b), but if $\mathbf{B} = a(1,-1,0)$ then they are absent (Fig. 4c). This is reflected in the LDOS maps in Fig. 4b,c. Here, there is no physical line connecting the two defects.

As elastic scattering by non-magnetic impurities cannot scatter electrons between the counterpropagating helical modes of the dislocation, they behave as ideal quantum wires at low temperatures, when inelastic processes are frozen out. This will have obvious consequences for electrical transport, although the challenge will be to separate this conduction mechanism from protected surface mode conduction, which is also present. In conduction across the short direction of anisotropic samples (for example, disc-shaped), dislocation-induced direct conduction paths should dominate over surface conduction. If dislocations can be induced in a controlled fashion during the growth process, then the direction-dependent condition for the existence of helical modes, and the dislocation density dependence of conductivity can be used to isolate this contribution. Another possibility is to introduce magnetic impurities on the surface of the insulator, which could potentially localize surface modes but have little impact on dislocation helical modes deep in the bulk. A rough estimate of the excess conductivity induced by dislocation modes for a dislocation density $n_d \sim 10^{12}\ \mathrm{m}^{-2}$ and a low-temperature scattering length $l \sim 1\,\mu\mathrm{m}$ along the dislocation[8] yields $\rho = (h/2e^2)(1/n_d l) \sim 10\,\mathrm{m}\Omega\,\mathrm{m}$, which should be experimentally accessible. It is conceivable that such novel quantum wires appearing within an insulating bulk medium, may be potentially relevant for spin and charge transport applications. A more exotic application might be to topological quantum computing for which a remarkable new architecture has recently been proposed, using vortex Majorana states confined at the interface between a conventional superconductor and a strong topological insulator[18]. Analogues of this proposal involving dislocations, rather than vortices, are worth exploring.

Methods

For a general topological insulator characterized by $\{\nu_0, \mathbf{M}_0\}$, and a dislocation with the Burgers vector $\mathbf{B}$, the condition for the existence of a protected 1D mode is given by equation (1) and derived below. First, let us briefly review the meaning of the topological insulator invariants $(\nu_0; \mathbf{M}_\nu)$. These are conveniently expressed in terms of quantities δ_i defined at the $i = 1 \ldots 8$ TRIMs of the 3D Brillouin zone, which can be computed for a given band structure[4]. However, these quantities depend in general on the gauge of the band wavefunctions, and are not directly meaningful. Certain products, however, are physically meaningful, such as $\prod_{i=1}^{8} \delta_i = (-1)^{\nu_0}$. One can use the gauge dependence to bring the δ_i into a simple form with the minimal number of TRIMs at which $\delta_i = -1$. For the strong topological insulator, one can arrange for a single negative value at precisely the TRIM $\mathbf{M}_\nu$, that is, $\delta_{\mathbf{M}_\nu} = -1$. For the weak topological insulator, there are necessarily two negative values, $\delta_{\mathbf{M}_\nu} = -1$ and $\delta_\Gamma = -1$, where $\Gamma = (0,0,0)$. Other physically meaningful combinations of the δ_i control properties of surface states that will be crucial for our purposes. Consider a crystal surface orthogonal to the reciprocal lattice vector $\mathbf{G}_3$. An important characteristic of the surface bands is the number of times they cross a generic Fermi energy that lies within the bulk gap, along a line in the Brillouin zone. In particular, the parity of the number of such band crossings (even versus odd) N_{cross}, when connecting two surface TRIMs $\mathbf{m}_1, \mathbf{m}_2$ is a topologically protected quantity related to the product[4]:

$$(-1)^{N_{\mathrm{cross}}} = \delta_{\mathbf{m}_1} \delta_{\mathbf{m}_2} \delta_{\mathbf{m}_1 + \frac{\mathbf{G}_3}{2}} \delta_{\mathbf{m}_2 + \frac{\mathbf{G}_3}{2}} \tag{3}$$

Consider now creating a screw dislocation in a general topological insulator with the Burgers vector $\mathbf{B}$. This is created using a cutting surface containing the dislocation—the surface is perpendicular to a reciprocal lattice vector, which we call $\mathbf{G}_3$. Atoms on one side of the surface are displaced by $\mathbf{B}$ and reconnected.

To derive the general condition for the existence of protected helical modes along the dislocation, we replay the analytical justification given previously for a specific model, for this more general case. A crucial step in that derivation was the fact that the surface states on the cut surfaces were Dirac nodes located at TRIMs. If an odd number of these modes acquire a π phase shift on creating the dislocation, a protected 1D mode results. Although in general, the surface band structure may be quite complicated, for the purpose of deriving robust topological properties one may adiabatically deform the crystal structure (during which the bulk gap remains open, and the Bravais lattice structure stays fixed). By this process, the surface modes can always be deformed into Dirac nodes that cross the bandgap, centred at the surface TRIMs. First, assume that the Burgers vector is a primitive lattice vector $\mathbf{B} = \mathbf{b}$, that is, it is the minimum-length lattice vector in that direction. We take the surface reciprocal lattice vectors to be $\mathbf{G}_1, \mathbf{G}_2$, with $\mathbf{G}_1 \cdot \mathbf{b} = 2\pi$ and $\mathbf{G}_2 \cdot \mathbf{b} = 0$. In addition, for a screw dislocation $\mathbf{b} \cdot \mathbf{G}_3 = 0$. The surface TRIMs are located at $\mathbf{m}_i \in \{\Gamma, (\mathbf{G}_1/2), (\mathbf{G}_2/2), (\mathbf{G}_1 + \mathbf{G}_2)/2\}$. Then, there are two surface TRIMs $\mathbf{m} = \{(\mathbf{G}_1/2), (\mathbf{G}_1 + \mathbf{G}_2/2)\}$ for which $\mathbf{B} \cdot \mathbf{m} = \pi(\mathrm{mod}\, 2\pi)$. If the number of surface Dirac nodes present in total at these two TRIMs N_{Dirac} is odd, then the dislocation will host a protected helical mode. Clearly, the parity of N_{Dirac} is related to the number of band crossings between the two surface TRIMs given by equation (3). Thus, the condition for the helical modes is

$$\delta_{\frac{\mathbf{G}_1}{2}} \delta_{\frac{\mathbf{G}_1+\mathbf{G}_2}{2}} \delta_{\frac{\mathbf{G}_1+\mathbf{G}_3}{2}} \delta_{\frac{\mathbf{G}_1+\mathbf{G}_2+\mathbf{G}_3}{2}} = -1$$

The product above can be simplified by going to the convenient gauge where only a single non-zero momentum TRIM has a negative δ, that is, $\delta_{\mathbf{M}_\nu} = -1$. Note, the defining property of the four TRIMs appearing in the product above is that $\mathbf{M} \cdot \mathbf{B} = \pi$. Hence, if the momentum $\mathbf{M}_\nu$ also satisfies this condition, then it appears in the product above, and the equation is satisfied. This leads us to the condition $\mathbf{B} \cdot \mathbf{M}_\nu = \pi(\mathrm{mod}\, 2\pi)$ for the existence of helical dislocation modes. In general, the Burgers vector is a multiple of the primitive lattice vector. If it is an odd multiple, the derivation above is unaffected. If, however, it is an even multiple, there are no dislocation modes because the phase shifts are always trivial. These more general cases are also captured by the formula above and hence we arrive at the general condition (1), for the existence of protected helical modes along the dislocation. Note, this derivation holds for both weak and strong topological insulators.

© 2009 Macmillan Publishers Limited. All rights reserved.

Received 21 October 2008; accepted 10 February 2009; published online 8 March 2009

References

1. Kane, C. L. & Mele, E. J. Quantum spin hall effect in graphene. *Phys. Rev. Lett.* **95**, 226801 (2005).
2. Kane, C. L. & Mele, E. J. Z_2 topological order and the quantum spin Hall effect. *Phys. Rev. Lett.* **95**, 146802 (2005).
3. Bernevig, B. A. & Zhang, S.-C. Quantum spin Hall effect. *Phys. Rev. Lett.* **96**, 106802 (2006).
4. Fu, L., Kane, C. L. & Mele, E. J. Topological insulators in three dimensions. *Phys. Rev. Lett.* **98**, 106803 (2007).
5. Moore, J. E. & Balents, L. Topological invariants of time-reversal-invariant band structures. *Phys. Rev. B* **75**, 121306 (2007).
6. Roy, R. Three dimensional topological invariants for time reversal invariant Hamiltonians and the three dimensional quantum spin Hall effect. Preprint at <http://arxiv.org/abs/cond-mat/0607531> (2006).
7. Bernevig, B. A., Hughes, T. L. & Zhang, S.-C. Quantum spin Hall effect and topological phase transition in HgTe quantum wells. *Science* **314**, 1757–1761 (2006).
8. Koenig, M. *et al.* Quantum spin Hall insulator state in HgTe quantum wells. *Science* **318**, 766–770 (2007).
9. Wu, C., Bernevig, B. A. & Zhang, S.-C. Helical liquid and the edge of quantum spin Hall systems. *Phys. Rev. Lett.* **96**, 106401 (2006).
10. Xu, C. & Moore, J. E. Stability of the quantum spin hall effect: Effects of interactions, disorder, and Z_2 topology. *Phys. Rev. B* **73**, 045322 (2006).
11. Hsieh, D. *et al.* A topological Dirac insulator in a quantum spin hall phase. *Nature* **452**, 970–974 (2008).
12. Fradkin, E., Dagotto, E. & Boyanovsky, D. Physical realization of the parity anomaly in condensed matter physics. *Phys. Rev. Lett.* **57**, 2967–2970 (1986).
13. Nakahara, M. *Geometry, Topology and Physics* (Institute of Physics, 2003).
14. Jackiw, R. & Rossi, P. Zero modes of the vortex-fermion system. *Nucl. Phys. B* **190**, 681–691 (1981).
15. Kohmoto, M., Halperin, B. I. & Wu, Y.-S. Diophantine equation for the three-dimensional quantum Hall effect. *Phys. Rev. B* **45**, 13488–13493 (1992).
16. Carpentier, D., LeDoussal, P. & Giamarchi, T. Stability of the Bragg glass phase in a layered geometry. *Europhys. Lett.* **35**, 379–384 (1996).
17. Teo, J. C. Y., Fu, L. & Kane, C. L. Surface states and topological invariants in three-dimensional topological insulators: Application to $Bi_{1-x}Sb_x$. *Phys. Rev. B* **78**, 045426 (2008).
18. Fu, L. & Kane, C. L. Superconducting proximity effect and majorana fermions at the surface of a topological insulator. *Phys. Rev. Lett.* **100**, 096407 (2008).

Acknowledgements

We acknowledge financial support from NSF DMR-0645691 and thank C. Kane and J. Orenstein for discussions.

Additional information

Reprints and permissions information is available online at http://npg.nature.com/reprintsandpermissions. Correspondence and requests for materials should be addressed to Y.R.

© 2009 Macmillan Publishers Limited. All rights reserved.